Fully atomistic modeling of an electric field poled guest-host nonlinear optical polymer

Won-Kook Kim and L. Michael Hayden[a)]
Department of Physics, University of Maryland, Baltimore County, Baltimore, Maryland 21250

(Received 16 November 1998; accepted 23 June 1999)

Fully atomistic molecular modeling is performed on an electric field poled guest-host nonlinear optical polymer system at two different densities. The higher density (HD) represents a sub-T_g system, while the lower density (LD) corresponds to a system above T_g. The electric field alignment of dopants was studied by calculating $\langle \cos\theta \rangle$ and $\langle \cos^3\theta \rangle$ and comparing with the theoretically predicted order parameters. For the LD system, the dipole orientational order achieved during 1.5 ns of NVT dynamics at 500 K was similar to the theoretical prediction. The applied field was also found to constrain the side group of the host, poly(methyl methacrylate) (PMMA). The shape of the volume swept by the dopants was found to be less cylindrical as the field was increased. The partial radial distribution functions indicated that the dopants were likely to be located near the host side group. No significant differences in the static conformational properties of the host were observed between poled and unpoled structures. In the HD system, the $COOCH_3$ side group motion was found to be more correlated with dopant orientation than the atoms in the backbone units. In the LD system, nearly equal side group and backbone contributions were involved in dopant orientation.
© *1999 American Institute of Physics.* [S0021-9606(99)51535-3]

INTRODUCTION

Nonlinear optical (NLO) polymeric materials have been extensively studied[1,2] for potential use in photonic applications, such as optical switches,[3] electro-optic (EO) modulators,[4,5] and high density optical data storage media,[6] due to their high intrinsic nonlinearities,[7] low dielectric constants, fast response times, ease-of-processibility, and low cost. Several types of polymeric NLO systems have been studied, including guest-host,[8–11] side-chain,[12,13] main-chain,[14,15] and cross-linkable systems.[16–18] The value of $\chi^{(2)}$, the second order optical susceptibility, in a given NLO system depends on the molecular hyperpolarizability β, the number of chromophores, and the degree of noncentrosymmetry. The last property can be attained by aligning chromophores via poling. Various poling methods have been demonstrated to achieve noncentrosymmetric dipole orientation such as corona poling,[19–21] contact poling,[22] and photo-induced poling.[23] Upon the removal of the poling source, the dipoles undergo thermal randomization, resulting in a decrease of $\chi^{(2)}$ with time.

The development of NLO polymer materials with simultaneous high nonlinearity and good thermal stability is the major impediment to marketing devices based on these materials. Understanding the physical mechanisms of chromophore orientation and/or re-orientation and the static properties of NLO polymers is essential to developing systems with high nonlinearity and excellent long term stability. There are many reports on the study of chromophore re-orientation using dielectric relaxation[24–27] or birefringence decay[24] in conjunction with second harmonic generation (SHG). As a result of these studies, and others, α-type relaxation associated with the glass transition has been proposed as the mechanism responsible for chromophore re-orientation.[24,28,29] However, most of these studies were carried out near or above the glass transition temperature, T_g. More recently, the influence of β-type relaxations on chromophore re-orientation in systems below T_g has been reported.[30–32] However, no conclusive evidence has been provided to elucidate the chromophore re-orientation mechanism at the molecular level.

Molecular modeling, using an empirically derived set of equations to describe the energy of a system as a function of atomic coordinates, has been applied to study the equilibrium properties as well as the kinetic physical properties for various polymer systems for a decade. Force field calculations such as these are required when the system size is too big to employ quantum mechanical calculations. From the detailed configurational coordinates, equilibrium properties such as solubility parameters,[33–35] conformational properties,[33–35] free volume distribution,[36–38] and time dependent properties such as polymer local dynamics[39–42] and small molecule diffusion[43–45] have been studied for several polymer systems. However, until now, no fully atomistic molecular dynamics have been employed to study the chromophore orientation mechanism in NLO polymers. Chromophore orientation under laboratory conditions, i.e., under moderate electric fields and temperatures, takes longer than nanoseconds to reach saturation, especially near or below T_g. This relatively long time scale can be a major handicap in utilizing molecular modeling, since simulation times longer than a few nanoseconds are not feasible with the present computational power. This difficulty can be relieved somewhat by introducing considerably larger electric fields and temperature to the system.[46]

[a)]Electronic mail: hayden@umbc.edu

 © 1999 American Institute of Physics

In this work, we used molecular modeling to investigate the static conformational properties, radial distribution functions, and energetics in poled and unpoled systems of poly(methylmethacrylate) (PMMA) doped with the NLO chromophore *N*,*N*-dimethyl-*p*-nitroaniline (DPNA). In addition, we studied the chromophore orientation process under the influence of an applied electric field. Eight independent molecular models of PMMA/DPNA at two different densities (HD and LD) were constructed and exposed to various electric fields. The higher density (HD) system corresponded to a sub-T_g state while the lower density (LD) system was above T_g. Since the local dynamics of PMMA below and above T_g are different, the polymer molecular motions correlated with chromophore alignment may also differ. Motivated by this possibility, we studied the effect of an applied electric field on the thermal fluctuations of the chromophores and the local dynamics of PMMA.

METHOD

The molecular dynamics and molecular mechanics in this study were performed using the molecular modeling package DISCOVER (4.0.0)[47] with the CVFF[48,49] force field (see the Appendix for the force field parameters). The potential energy in the simulations contains the following terms:

$$E = E_{\text{bond}} + E_{\text{angle}} + E_{\text{torsion}} + E_{\text{oop}} + E_{\text{nonbond}} + (E_{\text{field}}), \quad (1)$$

where E_{oop} is the energy term for the out-of-plane interactions, and E_{nonbond} comprises both the nonbonded van der Waals energy (E_{vdw}) and Coulombic (E_{Coul}) terms. E_{field} is the energy associated with the external electric field and was calculated from the summation of the dot products of the coordinates of each particle and the vector component of the product of the charge and the applied field,

$$E_{\text{field}} = \sum_{i=1}^{n} \mathbf{r}_i \cdot (q_i \mathbf{E}), \quad (2)$$

where i is the particle index. The E_{field} term is only included in the potential energy calculation during the poling stage. The electric field was applied in the z-direction for the simulation. The charge groups were properly assigned to be neutral for the simulation. A group-based nonbond energy calculation method was employed with 9.5 Å cut-off distance. In the group-based method, all atom pairs in the groups are included in the Coulombic interactions if the distance between the switching atoms of two groups is shorter than 9.5 Å. In this way, artifacts due to the splitting of dipoles can be efficiently prevented. The force field parameters, energy expressions, charges for the elements in the system, and the designation of the switch atoms that determine the groups in the group-based cut-off method are listed in the Appendix. Charges for the elements in the system, and the designation of the switch atoms that determine the group in the group based cut-off method are shown in Fig. 10. Four charge groups were assigned to the MMA units, CH_2, CH_3, C, and $COOCH_3$. Six charge groups were assigned to the DPNA molecules, -C(Ar)NO_2, -C(Ar)H, -C(Ar)H, -C(Ar)H, -C(Ar)H, and -C(Ar)N$(CH_3)_2$. The C(Ar) indicates a carbon atom in the phenyl ring of DPNA. The dipole moment of MMA calculated from the charges of the CVFF force field (1.7 D) is comparable to that obtained from the semiempirical molecular orbital program MOPAC (1.7–2.3 D). It should be pointed out that the dipole moment of DPNA calculated from the CVFF force field (3.84 D) is about a half of that calculated from MOPAC (~8 D). However, since the main goal of this work is to study the mechanism of dopant orientation qualitatively, use of the CVFF force field, which is one of the most widely tested and used force fields for organic molecules,[48,49] should not alter the results. Furthermore, since the orientation of the dipoles in the simulation is a function of the product of the dipole moment and the applied field, any degree of order can be obtained by the appropriate choice of the electric field parameter.

Each simulation box contained a single atactic (50:50 of meso:racemic ratios) PMMA chain with 90 repeat units and two DPNA molecules so that the mass fraction of the DPNA contents was 3%. Using a Monte-Carlo amorphous cell generation method,[50–52] eight independent initial HD structures were constructed in a cubic box, 23.60 Å on a side, resulting in a system density of 1.18 g/cm^3. These initial structures were further relaxed by 100 ps of NVT molecular dynamics (MD) simulation at 500 K, recording the configuration at every ps. The lowest potential energy snapshot was chosen and minimized further using a conjugate gradient method of 500 iterations with 0.1 kcal mol^{-1} Å^{-1} as the convergence criteria. At this stage, the potential energy of each isolated system was higher by a few hundred kcal than that of a bulk system, which is evidence that the molecular models were physically acceptable cohesive structures. In these initial structures, the orientations of the dopants were fairly random with the value of $\langle \cos\theta \rangle$ of -0.1, where θ is the angle between the applied field and the dopant dipole moment vector. The initial structures of the LD system were obtained by an additional 500 steps of energy minimization on the unpoled HD static structures with 0.1 kcal mol^{-1} Å^{-1} convergence in a cubic periodic box, 25.11 Å on a side. Due to the larger box size, the resulting LD density was 0.98 g/cm^3.

At 500 K, the HD system density of 1.18 g/cm^3 and the LD system density of 0.98 g/cm^3 correspond to a pressure of ~10,000 atm and ~1 atm, respectively, as verified using NPT dynamics. In other words, the HD and LD densities are the appropriate ones for this force field at 500 K and those two pressures. Furthermore, it is well known experimentally[53–55] that as pressure is applied to a polymeric system (hence increasing the density), the T_g increases. In fact, in PMMA, the T_g rises ~22 °C/1000 atm.[56] Therefore, we qualitatively identify our 500 K HD system as a sub-T_g system and the 500 K LD system as one above T_g.

The smaller size of the periodic box in the HD system provides less free space for the atoms to fluctuate and results in a higher internal pressure. For this reason, higher electric fields were needed to pole the chromophores in the HD system. Eight independent structures at each density were poled to attain sound statistics. NVT molecular dynamics were performed for 1.5 ns using a 1 fs time step and the velocity Verlet method.[57] The temperature of the system was controlled by a velocity scaling method[58] with temperature windows of 20 K around the target temperature of 500 K. Con-

figurational snapshots were recorded at every ps. The MD calculations were carried out on an SGI Challenge-XL server with 0.248 s/step of CPU time for the MIPS R10000 processor.

Two different types of poled static structures were also studied. These static structures were obtained through energy minimization of the lowest energy snapshot among 1500 recorded configurations from the two simulations with the highest order for each system density [50 kV/μm (HD), 5 kV/μm (LD)]. All 16 DPNA molecules were aligned fairly quickly at these fields and remained so with only a small amount of fluctuation for the rest of the simulation. For a meaningful comparison of the static properties of the systems, the equations of state for the systems should be identical. For this reason, both static molecular models were obtained at 1.18 g/cm^3. The same convergence criteria and number of iterations of energy minimization used to attain the unpoled static structures were employed to obtain the poled static structures in the HD system. The static structures poled from the LD system were obtained by employing two stages of minimization on the lowest energy snapshots of the trajectories, i.e., (i) 300 steps of energy minimization at 0.98 g/cm^3 and (ii) 500 steps of energy minimization at 1.18 g/cm^3, with 0.1 kcal mol^{-1} Å^{-1} convergence criteria and the conjugate gradient method.

RESULTS AND DISCUSSION

Static properties

To study the equilibrium properties in the static, poled and unpoled systems, we calculated the partial radial distribution functions between DPNA and PMMA and the rotational angle distributions in PMMA. Every static structure was found to be physically acceptable based on the energetics. Under the periodic conditions, the potential energy of the molecules was lower than that in a vacuum, which is evidence that the structure was cohesive. Poled static structures obtained from both the HD and LD systems were found to be less favored energetically than unpoled static structures. Also, the configurations poled from the LD system had a lower potential energy than those from the HD system. Nonbonded interaction energies of poled systems were considerably higher than that of an unpoled system, which indicates that poling results in poor molecular packing on the time scale of the simulation.

The orientational order parameter of the normals of two planes composed of two different side groups [$COOC(CH_3)$] in PMMA was calculated as a function of their separation distance. This calculation showed that the side units tend to be aligned parallel to each other at relatively short separation distances ($<\sim$5 Å) between the center of mass of the side units. This is further evidence that the initial static structure is well relaxed with no bad contacts between the side groups. This orientational correlation vanishes and the side groups align randomly for separation distances beyond $\sim$5 Å. This is similar to the orientational correlation that was found between two phenyl rings in several bulk aromatic polymer systems.[59,60]

The interaction between the DPNA chromophore and the PMMA matrix can be studied using the radial distribution function, which is defined as

$$G_{ab}(r)=\frac{\langle n_{ab}(r)\rangle}{4\pi r^2\,\Delta r\,\rho_{ab}}, \tag{3}$$

where $\langle n_{ab}(r)\rangle$ is the average number of atom pairs in a spherical shell located between r and $r+\Delta r$, and ρ_{ab} is the number density of atom pairs of type ab. In Fig. 1, the radial distribution functions of pairs of -NO_2 and sub-units in PMMA as well as -$N(CH_3)_2$ and sub-units in PMMA for unpoled systems, averaged over the eight structures, are shown. Only four sub-atomic units in PMMA were considered in $G(r)$: CH_2(ch2) units in the backbone, CH_3(bch3) units bonded to the backbone alpha carbon atom, the COO (coo) side group, and the CH_3(sch3) group bonded to oxygen. The coordinates of the center of mass of the atomic groups were employed and the minimum image convention periodic condition was used in the calculation of the separation distance between two pairs. The partial radial distribution functions reveal no appreciable order for relatively long separation distances (>6 Å), which is typical for an amorphous system. Figure 1 shows that the DPNA molecules have a higher chance to be located near the side units of PMMA based on broad and large peaks near $\sim$4 Å separation distance. For poled structures, a similar behavior was found.

The torsional angles of PMMA are defined in Fig. 2. The

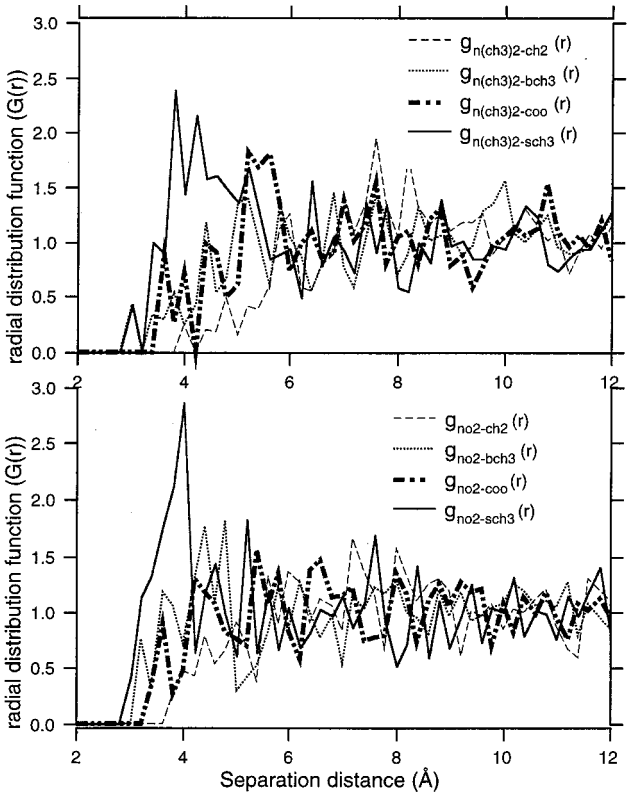

FIG. 1. Partial radial distribution functions between the center of mass of $N(CH_3)_2$ in DPNA and sub-units in PMMA and those between the center of mass of NO_2 in DPNA and sub-units in PMMA in unpoled static structures. DPNA molecules are likely to be surrounded by the $COOCH_3$(sch3) side group. Similar behavior was observed for poled systems as well.

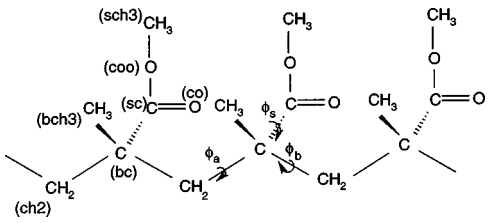

FIG. 2. Definitions of torsional angles and the atom types in PMMA. ϕ_a, ϕ_b, and ϕ_s are the torsional angles of CH_2-C-CH_2-C, C-CH_2-C-CH_2, and CH_2-C-C-O(CH_3) bonds, respectively.

torsional angle distributions of the PMMA bonds are shown in Fig. 3. The torsional angle of the C–O bond was not considered since the ester group is rigid and planar by nature. For all torsional angles, fairly symmetric distributions were attained due to the random distributions of meso and racemic isomers. For all three structures, three torsional states were highly populated near trans, gauche, and anti-gauche for both ϕ_a and ϕ_b backbone bonds as suggested by Sundararajan.[61] No significant differences in the distributions of backbone torsional angles could be found between poled and unpoled structures. The overall PMMA parent chain dimension in terms of mean square end-to-end distance and radius of gyration did not show considerable difference for the three static structures either. Distributions of ϕ_s are fairly broad with dense populations near $-60°$ and $60°$. The ϕ_s is defined

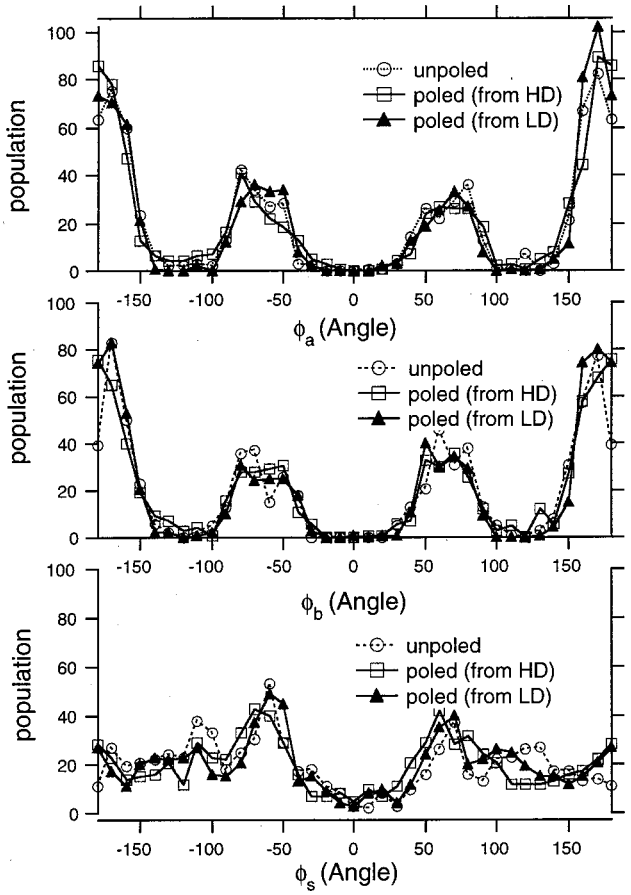

FIG. 3. Torsional angle distributions of PMMA molecules for both unpoled and poled systems. No significant differences in torsional distributions of backbone bonds were observed.

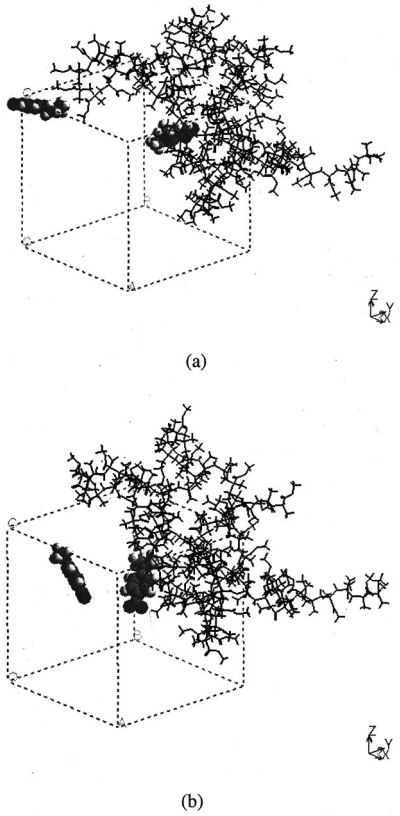

FIG. 4. Snapshots of the LD molecular system. A 5 kV/μm electric field was applied in the *z*-direction. The DPNA molecules are shown in the ball style. (a) At the start of the simulation, the DPNA molecules were not aligned to the field direction. (b) At the end of the simulation, the DPNA molecules were well aligned with the applied field.

differently from that normally found in the literature[61,62] as the description of the torsional angle of the side unit in PMMA. In our definition of ϕ_s, when the plane of the carbonyl group is perpendicular to the plane defined by adjoining skeletal backbone bonds, orientations $\phi_s = -60°(d)$ or $60°(l)$ were assigned. Only slight differences can be found in the distributions of ϕ_s between poled and unpoled structures.

Dopant orientation

The final orientation of the DPNA molecules are affected not only by the applied field and bulk temperature but also by the local environment surrounding them, such as the local dynamics of the polymer matrix and the free volume size and shape near the chromophore. Therefore, the classical statistical treatment of dipole orientational ordering,[63] which is based on an ideal gas like system and does not include the local polymer mobility or the surroundings of the chromophore, may not be sufficient to predict the dipole orientational order and eventually the susceptibility such as $\chi^{(2)}_{zxx}$ and $\chi^{(2)}_{zzz}$. To elucidate this difficulty, we performed MD on a PMMA/DPNA guest-host NLO system under various applied electric field strengths at two different densities. For the HD system, we applied fields of 5 kV/μm, 10 kV/μm, and 50 kV/μm, while, for the LD system, we used fields of 0.5 kV/μm, 1 kV/μm, and 5 kV/μm. In Fig. 4, two snapshots

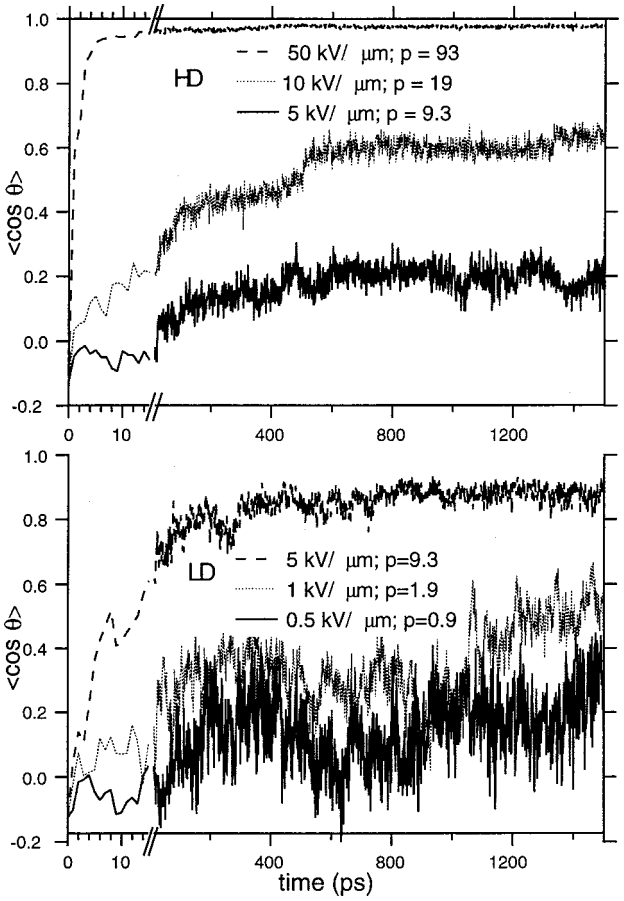

FIG. 5. The average value of the dipole moment vector of DPNA along the field direction with respect to poling time for the HD (1.18 g/cm^3) and LD (0.98 g/cm^3) systems, respectively. The average value was obtained from 16 DPNA molecules.

of one of the LD systems are shown. At the beginning of the simulation, the DPNA molecules are randomly aligned to the field direction, but once the field is applied, the dopants rotate fairly well and maintain their orientation until the simulation ends.

The orientation of a collection of dipoles can be described using odd-order Langevin functions such as $L_1(p)$ or $L_3(p)$, which correspond to $\langle\cos\theta\rangle$ or $\langle\cos^3\theta\rangle$, respectively. Here θ is the angle between the electric field vector and molecular dipole vector, and p is equal to $\mu E/kT$, where μ is the dipole moment, E is the electric field, k is Boltzmann's constant, and T is the absolute temperature. The statistical thermodynamics of electric field induced dipole alignment for $\langle\cos\theta\rangle$ and $\langle\cos^3\theta\rangle$ can be described in terms of the parameter p as[64]

$$\langle\cos\theta\rangle = \coth p - 1/p = L_1(p), \tag{4}$$

$$\langle\cos^3\theta\rangle = L_3(p) = \left(1+\frac{6}{p^2}\right)L_1(p) - \frac{2}{p}. \tag{5}$$

The above equations predict saturation of the field induced dipole alignment near unity for sufficiently large values of p.

The field induced alignment of DPNA is shown in Fig. 5. Relatively rapid saturation of the dopant alignment was obtained for the 50 kV/μm field in the HD system as well as the 5 kV/μm field in the LD system. Values for $\langle\cos\theta\rangle$ and $\langle\cos^3\theta\rangle$ were calculated from the last 100 ps of the trajectories and are listed in Table I with their standard deviation of the mean and compared with $L_1(p)$ and $L_3(p)$ predicted from Eqs. (4) and (5). For the dipole moment of DPNA, the partial charges in the CVFF force field were employed. For this reason, the local field effect is ignored in the calculation of μ. Only at the highest field is there agreement between $\langle\cos\theta\rangle$ and $L_1(p)$ as well as between $\langle\cos^3\theta\rangle$ and $L_3(p)$ for the HD system. However, for the LD system, good agreement is found for much lower fields. Based on the comparison between $\langle\cos\theta\rangle$ and $L_1(p)$, the time required to reach saturation of the dipole orientation decreases with increasing field strength for a given density (or pressure) and increases with increased density (or increased pressure) for a given field strength. Nevertheless, the time required to reach saturation may be longer than the nanosecond time scale unless the applied field is considerably high or the density of the system is low. A great difference in order between the HD and LD systems for the 5 kV/μm field is noticeable, indicating that chromophore orientation is greatly influenced by polymer mobility. The results are in good qualitative agreement with extensive NLO experiments in poled polymers performed over the last 10 years including those that carefully examined the poling procedure itself.[8,20,21,65]

The mobility of polymers can be studied using the Torsional Auto Correlation Function (TACF) which can be defined as[41]

$$G(t) = \langle\cos[\phi(t) - \phi(0)]\rangle, \tag{6}$$

TABLE I. A comparison of $\langle\cos\theta\rangle$ and $\langle\cos^3\theta\rangle$ calculated from the last 100 ps of MD trajectories with the theoretical predictions of $L_1(p)$ and $L_3(p)$, where p is equal to $(\mu E/kT)$. The dipole moment μ of DPNA was calculated from the partial charges assigned by the CVFF force field. ($\mu = 3.84$ D).

	0.5 kV/μm	1 kV/μm	5 kV/μm	10 kV/μm	50 kV/μm
p $(\mu E/kT)$	0.9	1.9	9.3	19	93
HD					
$\langle\cos\theta\rangle$	-	-	0.18±0.01	0.64±0.01	0.98±0.00
$\langle\cos^3\theta\rangle$	-	-	0.04±0.01	0.47±0.01	0.93±0.00
LD					
$\langle\cos\theta\rangle$	0.21±0.02	0.53±0.02	0.88±0.01	-	-
$\langle\cos^3\theta\rangle$	0.13±0.01	0.33±0.02	0.71±0.01	-	-
$L_1(p)$	0.29	0.51	0.89	0.95	~1.0
$L_3(p)$	0.18	0.31	0.74	0.86	~1.0

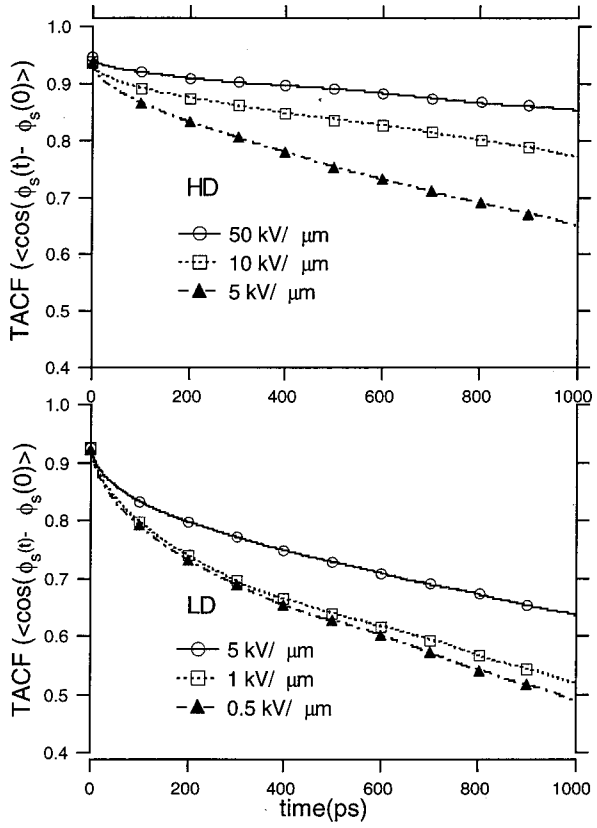

FIG. 6. Torsional auto correlation function of the ϕ_s bond in PMMA for the HD and LD system. As the field strength increases, the TACF of ϕ_s decays more slowly.

where the angle bracket represents averaging over all possible time origins. For the LD system, the TACFs of backbone bonds decayed faster than in the HD system indicating that backbone bonds have a better chance of a rotational transition than those in the HD system. For the rotational motion of ϕ_s bonds, a relatively small amount of free space is required compared to the backbone bonds, therefore the density does not effect the rotational motion of the side group as much as for the rotational motion of backbone bonds. TACFs were also studied as variables of field strength for both the HD and LD system. The field dependence of the TACFs of ϕ_s is shown in Fig. 6. The TACFs decay more slowly as the field is increased. A similar trend was observed for both ϕ_a and ϕ_b, but the field dependence of the backbone bonds was weaker. In fact, the field dependence of the backbone bond motion was nearly negligible for the HD system. Due to the dipoles in the $-COOCH_3$ unit, the side group torsional motion is more significantly affected by fields than the backbone bonds.

To study chain end effects, each unit was numbered from the head or tail unit. Units of $i<4$ are six of three successive ones from head or tail, units of $i>5$ are 80 units in the chain middle which are separated by more than 5 units from the head or tail. Head and tail units were found to align faster than chain middle units for a given field. But, nearly similar alignment was found between chain ends and chain middle units at the simulation end. For the PMMA host, the difference between $\langle \cos\theta \rangle$ and $L_1(p)$ was found to be smaller for lower fields and larger for higher fields which is opposite to that for the dopants. Since the PMMA unit is not a rigid shape, the monomer dipole moment can fluctuate due to small geometrical adjustments and small amplitude rotational motions within a single torsional barrier. Moreover, the PMMA unit is more hindered than the dopant, and hence requires relatively long range cooperative motions along the chain backbone to orient. For this reason, less alignment of PMMA units is obtained than for DPNA.

DPNA molecular motion and the electric field effects

Once the electric field is applied to the system, molecular motion is no longer random. Local motions are influenced by the field. To study this effect, we studied the shape and the size of the total swept volume of the DPNA molecule as a function of field strength.

The shape and size of the volume swept by the DPNA molecule were studied by employing a hard sphere diameter of atoms and cubic subcells. The hard sphere diameter of atoms was chosen to be $0.89R_0$ where R_0 is the van der Waals radius determined from the CVFF force field. The simulation box was divided into cubic subcells of size 0.4 Å. Each grid was scanned and categorized as to whether it was visited by any atom of the DPNA molecule during the 1.5 ns trajectory. Whenever more than half of the subcell lays within any hard sphere, the address (coordinate) of the subcell was recorded. The shape of the swept volume was analyzed using the principal moments of the radius of gyration tensor.[66–68] Asphericity (σ) and acylindricity (χ) can be measured by using three eigenvalues P_1^2, P_2^2, and P_3^2 of the radius of gyration tensor where the eigenvalues were sorted in the order of $P_1^2 \geqslant P_2^2 \geqslant P_3^2$.[69] The square of the radius of gyration (s^2) is the sum of P_1^2, P_2^2, and P_3^2. $\sigma(\geqslant 0)$ and $\chi(\geqslant 0)$ can be defined as

$$\sigma = P_1^2 - \frac{(P_2^2 + P_3^2)}{2} \tag{7}$$

and

$$\chi = P_2^2 - P_3^2. \tag{8}$$

The lower limit of σ is for tetrahedral or higher symmetry; for other shapes $\sigma > 0$. The lower limit for χ is for cylindrical symmetry; for other shapes $\chi > 0$. The relative shape anisotropy is

$$\kappa^2 = \frac{(\sigma^2 + (3/4)\chi^2)}{s^4}, \tag{9}$$

with $0 \leqslant \kappa^2 \leqslant 1$. The lower limit is achieved for a structure of tetrahedral or higher symmetry and the upper limit is for a linear array.[69]

In Fig. 7, the swept volume of one DPNA molecule is visualized for both HD and LD systems. The initial starting structure is nearly equivalent for each except for slight differences of atomic position resulting from an additional energy minimization for the LD system. Under the minimum image convention used in the periodic boundary conditions, the increase of the periodic box size to attain the system density of 0.98 g/cm^3 results in an increase of the separation

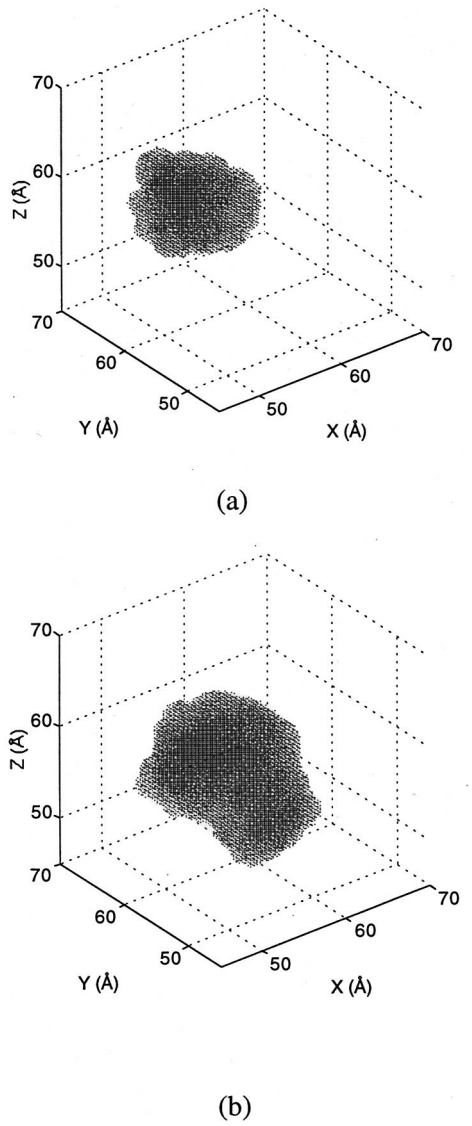

FIG. 7. Visualization of the total swept volume of one DPNA molecule during 1.5 ns for the (a) HD and (b) LD systems for 5 kV/μm.

for atom pairs having attractive interaction and separated by larger than half of the HD system periodicity. This increase in separation distance raises the interaction energy of the pair, hence, an additional energy minimization is necessary. No significant translational diffusion for 1.5 ns at 500 K can be observed for either system, but the swept volume size of the LD system is larger than that of the HD system, as expected. Values of $\langle s^2\rangle$, $\langle\sigma\rangle/\langle s^2\rangle$, $\langle\chi\rangle/\langle s^2\rangle$, and $\langle\kappa^2\rangle$ and their standard deviations of the means are listed in Table II for various fields. Table II shows that as the field is increased, the shape of the swept volume is less cylindrical for both systems. As the field increases, DPNA can change its orientation more significantly. Due to this large orientational change, the swept volume shape deviates from the rod like DPNA molecular shape. For the LD system, the swept volume size decreases as the field increases, as a result of the constrained thermal motion due to the introduction of the applied field. At the common field of 5 kV/μm, the swept volume of the LD system is less cylindrical and more spherical than that of the HD system. The extra free volume in the

TABLE II. Asymmetry analysis of the volume swept by DPNA during 1.5 ns of poling. The amount of swept volume for the LD system is almost twice that of the HD system due to the greater accessible volumes in the system. For the LD system, the amount of swept volume decreases as the field increases. As the field increases, the acylindricity increases.

	$\langle s^2\rangle$	$\langle\sigma\rangle/\langle s^2\rangle$	$\langle\chi\rangle/\langle s^2\rangle$	$\langle\kappa^2\rangle$
HD system				
50 kV/μm	29±1	0.40±0.02	0.13±0.01	0.17±0.02
10 kV/μm	25±1	0.35±0.03	0.11±0.02	0.13±0.02
5 kV/μm	26±1	0.43±0.03	0.09±0.01	0.19±0.02
LD system				
5 kV/μm	47±3	0.38±0.03	0.12±0.02	0.15±0.02
1 kV/μm	53±2	0.36±0.03	0.12±0.02	0.14±0.02
0.5 kV/μm	58±5	0.46±0.05	0.08±0.02	0.20±0.04

LD system allows more random thermal motion which results in a more spherical shape than cylindrical shape, and for this reason, the relative asymmetry of the swept volume, $\langle\kappa^2\rangle$ of the LD system is less than that of the HD system.

Detailed analysis of DPNA orientation

In the LD system, the rotational motion of each DPNA molecule involves a few ''large'' jumps (i.e., $\Delta\theta \geqslant 0.5$ rad or $\sim\pi/6$), which occur in a fairly short time period as can be seen in Fig. 8. The HD system is similarly characterized except that the ''large'' jumps are less frequent and have smaller angular displacements in general. A comparison of the incidence of these large jumps to the value of the projection of the molecular dipole moment along the field direction ($\cos\theta$ in Fig. 8), for a single dopant molecule, during the same time period reveals a qualitative correspondence. During periods of relatively small angular displacements (near

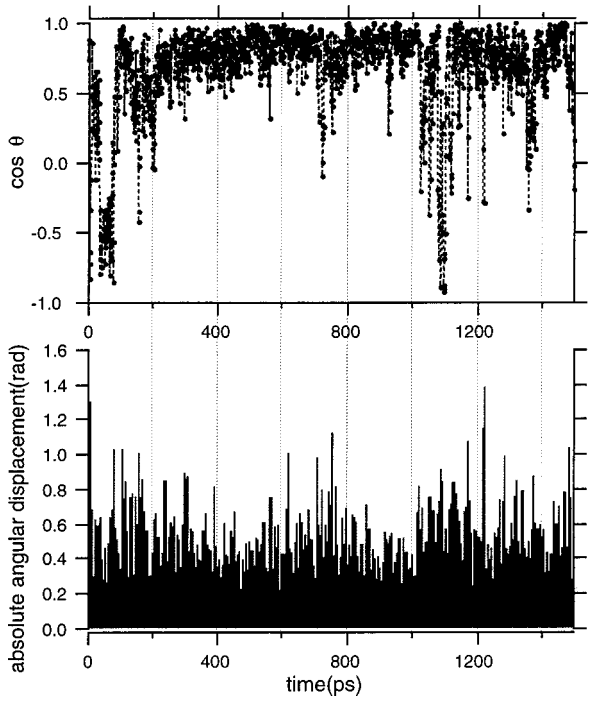

FIG. 8. A comparison between the absolute angular displacement of a DPNA molecule in the LD system with 1 kV/μm of the applied field and the projection of the molecular dipole moment along the field direction.

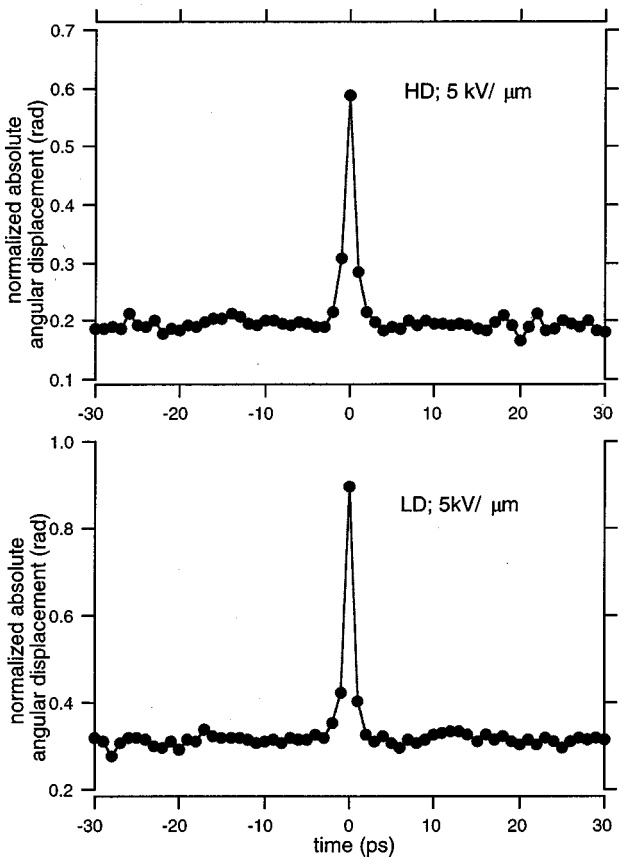

FIG. 9. Normalized absolute angular displacement of DPNA with 5 kV/μm of the field for both the HD and the LD systems. $t=0$ ps is the time frame when the absolute angular displacement of DPNA is greater than $\pi/6$ and $\pi/4$ for the HD and the LD system, respectively.

500 ps and 950 ps), $\cos\theta$ is relatively constant. However, during periods of large angular displacements (near 100, 750, and 1050–1300 ps), $\cos\theta$ exhibits large fluctuations. A model that accounts for these results is that the dopant orientation occurs chiefly through these relatively big rotational jumps rather than by a process consisting of many incremental motions. A corresponding analysis of the absolute translational displacement of the dopant showed that during the field induced orientation, the dopant translational jumps were only 1–2 Å, suggesting that the orientation process is effected only by the dopant's immediate environment. This is in contrast to the observation by Hall *et al.*, that, during the average dopant reorientation time, near T_g, the dopant can translate (via diffusion) over 70 times its length.[70] These studies of the translation–rotation paradox by Hall *et al.* showed that reorientation times and diffusion times near T_g are very different, with reorientation times being much longer. Our simulation data suggests that the application of an electric field significantly decreases the orientational relaxation time such that little diffusion is seen during that time. These results clearly point out the difference between orientation and reorientation and point to the need for future molecular modeling studies of the reorientation process.

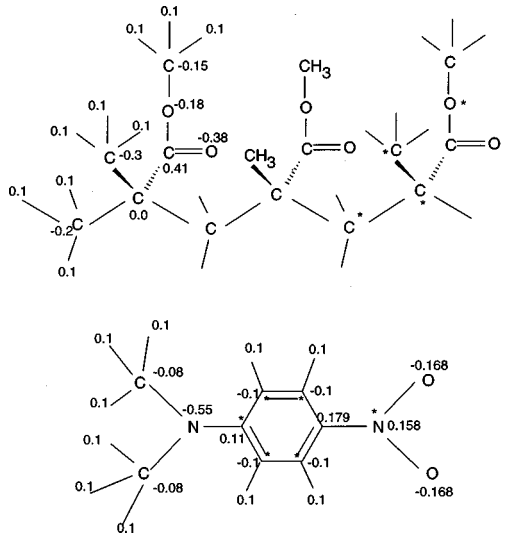

FIG. 10. Coulombic interaction: ${}^{+}E_{\mathrm{Coul}}=q_iq_j/r_{ij}^{+}$ The assigned charges, q_i for the elements on the PMMA and the DPNA molecules are shown below. The unit of the charge is $e(1.6\times10^{-19}\,^{\circ}\mathrm{C})$ and the atoms marked with* are the switch atoms for the charge groups.

TABLE III. The ratios of the normalized absolute distribution of atoms between region I and region II, when DPNA experiences a relatively big rotational jump. Atom types with higher values are more correlated to the motion of the DPNA dopant. For the HD system, the motion of the $COOCH_3$ side groups can be considered to be more correlated with DPNA orientation, while for the LD system, motions of all atom types contribute nearly equally to DPNA orientation.

	HD (5 kV/μm)	LD (5 kV/μm)
bch3	1.08±0.10	1.06±0.02
ch2	1.06±0.10	1.06±0.03
bc	1.08±0.10	1.04±0.02
sch3	1.13±0.11	1.07±0.01
sc	1.11±0.10	1.05±0.01
coo	1.12±0.11	1.07±0.01
co	1.13±0.10	1.07±0.01

To examine our model further, we analyzed the time scale of the rotational jumps of DPNA and tried to identify the molecular motions in PMMA which appeared to be most correlated with a rotational jumping event. The absolute angular displacement at every ps and the center of mass positions of the NO_2 and $N(CH_3)_2$ units in each DPNA molecule were found. When the absolute angular displacement for a given time frame was greater than $\Delta\theta_c$, where $\Delta\theta_c$ is an arbitrarily chosen critical angular displacement ($\Delta\theta_c=\pi/6$ for HD, and $\Delta\theta_c=\pi/4$ for LD), then a rotational jumping event was assumed and the corresponding time frame was recorded. The selection of these critical values ensured that we included only the largest jumps in each system. In the LD system, the rotational fluctuation of dopants was relatively higher, therefore a higher $\Delta\theta_c$ was employed. A few hundred rotational jumping events were found for the 16 DPNA molecules for simulations in the HD system and about twice as many events were found for the LD system. To study the time scale of rotational jumping, absolute angular displacements of the previous 30 ps and the next 30 ps were recorded and accumulated for the each rotational jump event. The accumulated displacements were then normalized with their frequencies. In Fig. 9, the normalized angular displacements around the jump event are shown for both systems. In both

the HD and LD systems, the normalized angular displacements very near the rotational jumping event (for instance, between ± 1 ps) are slightly higher than those from relatively long time intervals from the jumping event ($|t| > \sim 4$ ps). This indicates that the rotational jumping event of DPNA takes 3–5 ps. No significant field effects on the time scale of a jumping event were observed.

We also calculated the absolute displacement of the atoms in the polymer at every rotational jumping event as a function of their location from DPNA. Region I was assigned for the atoms located within 6 Å from the center of mass of either the NO_2 or $N(CH_3)_2$ units, otherwise, region II is assigned. The absolute displacement was accumulated for each atom type and then normalized by their populations. The ratios of the normalized displacements of the atoms between region I and region II were calculated and are listed in Table III. Hydrogen atoms were excluded in the lists. The relatively large standard deviations of the mean for the HD system may be related with the different surroundings near the dopants at the beginning of the simulation and less frequent rotational jumping events. Atom types with higher values are more correlated with the motions of the DPNA dopants. Every type of atom in region I had a higher absolute displacement than those in region II for both the HD and LD systems. For the HD system, which is in a sub-T_g state, the motion of the side group $COOCH_3$ unit is more correlated with DPNA orientation, while in the LD system, which is above T_g, motions of all atom types have nearly equal contributions to DPNA orientation. These results are in agreement with the arguments suggested by experimental work on sub-T_g states[30–32] using SHG and EO techniques.

CONCLUSIONS

We performed a molecular modeling study on a PMMA/DPNA guest-host NLO system at two different densities to investigate the chromophore orientation process in the presence of an applied electric field. The static properties were also studied for both unpoled structures and structures poled from HD and LD systems in terms of energetics, partial radial distribution functions, and torsional angle distributions. The unpoled systems were found to be energetically more stable than the poled system. DPNA molecules were more likely to be located near the side group than backbone units for all structures and no significant differences in conformational properties between poled and unpoled systems were observed. The orientational order was calculated using $\langle \cos\theta \rangle$ and $\langle \cos^3\theta \rangle$ for both HD and LD systems and compared to theoretically predicted $L_1(p)$ and $L_3(p)$ for various fields. The calculated $\langle \cos\theta \rangle$ and $\langle \cos^3\theta \rangle$ from LD systems were similar to the theoretical prediction for a noninteracting rigid gas. For identical fields, the alignment process was considerably slower in the HD system compared to the LD system.

Torsional auto correlation functions of PMMA at both densities were calculated for various fields. The field was found to affect the local dynamics of the PMMA molecules and eventually constrains torsional fluctuations somewhat. This effect was more significant for rotational motions of the side group. However, the field strength in the simulation is unrealistically high, therefore it may not be easy to observe the constrained local motions of PMMA experimentally. The shape of the dopant swept volume was also affected by the field. As the field was increased, the dopant swept volume shape changed toward a disk like shape from a rod like shape.

We also attempted to distinguish which part of the motion in PMMA is mainly correlated with the DPNA orientation. A higher absolute displacement of atoms in $COOCH_3$ side groups in the HD system lead us to conclude that the $COOCH_3$ side group motion is more correlated with chromophore orientation than backbone units when below T_g. Above T_g(LD), nearly equal contributions of backbone and side group atoms were involved in chromophore orientation.

ACKNOWLEDGMENTS

This material is based on work supported by the National Science Foundation under Grant No. DMR-9705800. The authors thank Dr. Kung for helpful discussions on btcl scripts for the E_{field} calculation.

APPENDIX

Geometry and energy expressions for the simulations are shown in the following table:

Bond length: $E_{\text{bond}} = K_l(R - R_0)^2$	R_0 (Å)	K_l (kcal/mol Å^2)
C–N	1.460	377.575
N′–O	1.218	560.994
C(Ar)–N	1.420	280.000
C(Ar)–N′(NO_2)	1.472	351.253
C–H	1.105	340.618
C(Ar)–H	1.080	363.416
C(Ar)–C(Ar)	1.340	480.000
C–C	1.526	322.716
C–C′(COO)	1.520	283.092
C′–O′(C=O)	1.230	615.322
C′–O	1.370	400.000
O–C	1.425	273.200

Bond angle: $E_{\text{angle}} = K_\theta(\theta - \theta_0)^2$	θ_0 (degrees)	K_θ [kcal/(mol rad^2)]
C–N–C	120.0	37.000
C–N–C(Ar)	120.0	50.000
H–C–N	109.5	51.500
H–C(Ar)–C(Ar)	120.0	37.000
C(Ar)–C(Ar)–C(Ar)	120.0	90.000
C(Ar)–C(Ar)–N	120.0	102.000
C(Ar)–C(Ar)–N′	120.0	34.680
C(Ar)–N′–O^-	120.0	54.500
O^-–N′–O^-	120.0	113.573
C–C–C	110.5	46.600
C–C–C′	110.5	46.600
C–C′–O	110.0	122.800
C–C′–O′	120.0	68.000
H–C–H	106.4	39.500
H–C–C	110.0	44.400
O′–C′–O	123.0	145.000
C′–O–C	109.5	60.000
H–C–O	109.5	57.000

Torsion: $E_{tor}=K_{\phi}[1+\cos(n\phi-\phi_0)]$

	K_{ϕ} (kcal/mol)	n	ϕ_0 (degrees)
X–N–C–X	0.000	0	0.000
X–C(Ar)–N–X	10.000	2	180.000
C(Ar)–C(Ar)–N′–O$^-$	10.000	2	180.000
X–C(Ar)–C(Ar)–X	12.000	2	180.000
X–C–C–X	1.423	3	0.000
C–C–C′–O′	10.000	2	180.000
C–C–C′–O	0.00	0	0.000
C′–O–C–H	0.39	3	0.000
O′–C′–O–C	4.5	2	180.000

Out-of-plane:[a] $E_{oop}=K_{\chi}[1+\cos(n\chi-\chi_0)]$

	K_{χ} (kcal/mol)	n	χ_0 (degrees)
O$^-$–N′–O$^-$–C(Ar)	10.00	2	180.00
C(Ar)–C(Ar)–C(Ar)–*X*	0.37	2	180.00
C(Ar)–N–C–C	0.05	2	180.00
C(Ar)–C(Ar)–C(Ar)–N′	10.00	2	180.00
C–C′–O′–O	11.60	2	180.00

[a]The out-of-plane is defined as a torsion of A1–A2–A3–A4 where A2 is a central atom and A3–A4 is not a real bond.

van der Waals (12-6): $E_{vdw}=A_{ij}/r^{12}-B_{ij}/r^6$ where $A_{ij}=\sqrt{A_iA_j}$, $B_{ij}=\sqrt{B_iB_j}$

Atom type	A_{ij} [kcal/(mol Å^{12})]	B_{ij} [kcal/(mol Å^6)]
C(CH$_3$)	1790340.7240	528.48190
C(CH$_2$)	1790340.7240	528.48190
C	1790340.7240	528.48190
C(Ar)	2968753.3590	1325.7081
C′	2968753.3590	1325.7081
O′	272894.7846	498.8788
O	272894.7846	498.8788
N	2266872.4000	1230.5570
N′	2266872.4000	1230.5570
O$^-$	272894.7846	498.8788
H	7108.4660	32.8708

[1] C. S. Willand and D. J. Williams, Ber. Bunsenges. Phys. Chem. **91**, 1304 (1987).
[2] G. A. Lindsay and K. D. Singer, *Polymers for Second Order Nonlinear Optics* (American Chemical Society, Washington DC, 1995).
[3] G. H. Cross, A. Donaldson, R. W. Gymer, S. Mann, N. J. Parsons, D. R. Haas, H. T. Man, and H. N. Yoon, Proc. SPIE **79**, 1177 (1989).
[4] P. Kaczmarski, J.-P. Van de Capelle, P. E. Lagasse, and R. Meynart, IEE Proc.: Optoelectron. **136**, 152 (1989).
[5] R. Dagani, Chem. Eng. News **74**, 20 (1996).
[6] C. A. Eldering, S. T. Kowel, P. Brinkley, N. Matloff, T. Schubert, and R. Gosula, Proc. SPIE **72**, 1151 (1989).
[7] A. Buckely, Adv. Mater. **4**, 153 (1992).
[8] H. L. Hampsch, J. Yang, G. K. Wong, and J. M. Torkelson, Macromolecules **23**, 3648 (1990).
[9] J. W. Wu, J. F. Valley, S. Ermer, E. S. Binkley, J. T. Kenney, G. F. Lipscomb, and R. Lytel, Appl. Phys. Lett. **58**, 225 (1991).
[10] A. Dhinojwala, G. K. Wong, and J. M. Torkelson, Macromolecules **25**, 7395 (1992).
[11] S. C. Brower and L. M. Hayden, Appl. Phys. Lett. **63**, 2059 (1993).
[12] H.-T. Man and H. N. Yoon, Adv. Mater. **4**, 159 (1992).
[13] T. Verbiest, D. M. Burland, M. C. Jurich, V. Y. Lee, R. D. Miller, and W. Volksen, Science **268**, 1604 (1995).
[14] I. Teraoka, D. Jungbauer, B. Reck, D. Y. Yoon, R. Twieg, and C. G. Willson, J. Appl. Phys. **69**, 2568 (1991).
[15] C. Xu, B. Wu, L. R. Dalton, P. M. Ranon, Y. Shi, and W. H. Steier, Macromolecules **25**, 6716 (1992).
[16] D. Jungbauer, B. Reck, R. Twieg, D. Y. Yoon, C. G. Willson, and J. D. Swalen, Appl. Phys. Lett. **56**, 2610 (1990).
[17] M. Chen, L. R. Dalton, L. P. Yu, Y. Q. Shi, and W. H. Steier, Macromolecules **25**, 4032 (1992).
[18] M. E. Wright, I. E. McFarland, L. M. Hayden, and S. C. Brower, Macromolecules **28**, 8129 (1995).
[19] K. D. Singer, M. G. Kuzyk, W. R. Holland, J. E. Sohn, S. J. Lalama, R. B. Comizzoli, H. E. Katz, and M. L. Schilling, Appl. Phys. Lett. **53**, 1800 (1988).
[20] M. Eich, A. Sen, H. Looser, G. C. Bjorklund, J. D. Swalen, R. Twieg, and D. Y. Yoon, J. Appl. Phys. **66**, 2559 (1989).
[21] A. Knoesen, N. E. Molau, D. R. Yankelevich, M. A. Mortazavi, and A. Dienes, Int. J. Nonlinear Opt. Phys. **1**, 73 (1992).
[22] C. H. Wang, S. H. Gu, and H. W. Guan, J. Chem. Phys. **99**, 5597 (1993).
[23] P. M. Blanchard and G. R. Mitchell, Appl. Phys. Lett. **63**, 2038 (1993).
[24] D. Jungbauer, I. Teraoka, D. Y. Yoon, B. Reck, J. D. Swalen, R. Tweig, and C. G. Wilson, J. Appl. Phys. **69**, 8011 (1991).
[25] M. S. Dionisio, J. J. Moura-Ramos, and G. Williams, Polymer **35**, 1705 (1994).
[26] A. Dhinojwala, G. K. Wong, and J. M. Torkelson, J. Chem. Phys. **100**, 6046 (1994).
[27] A. Dhinojwala, J. C. Hooker, and J. M. Torkelson, J. Non-Cryst. Solids **172**, 286 (1994).
[28] W. Kohler, D. R. Robello, P. T. Dao, C. S. Willand, and D. J. Williams, J. Chem. Phys. **93**, 9157 (1990).
[29] A. Dhinojwala, G. K. Wong, and J. M. Torkelson, Macromolecules **26**, 5943 (1993).
[30] F. Ghebremichael, M. G. Kuzyk, and C. W. Dirk, Nonlinear Opt. **6**, 123 (1993).
[31] S. J. Strutz, S. C. Brower, and L. M. Hayden, J. Polym. Sci., Part B: Polym. Phys. **36**, 901 (1998).
[32] F. Ghebremichael and H. S. Lackritz, Appl. Opt. **36**, 4081 (1997).
[33] D. N. Theodorou and U. W. Suter, Macromolecules **18**, 1467 (1985).
[34] M. Hutnik, A. S. Argon, and U. W. Suter, Macromolecules **24**, 5970 (1991).
[35] Y. Li and W. L. Mattice, Macromolecules **25**, 4942 (1992).
[36] D. Rigby and R. J. Roe, Macromolecules **23**, 5312 (1990).
[37] M. L. Greenfield and D. N. Theodorou, Macromolecules **26**, 5461 (1993).
[38] S. Misra and W. L. Mattice, Macromolecules **26**, 7274 (1993).
[39] D. B. Adolf and M. D. Ediger, Macromolecules **24**, 5834 (1991).
[40] H. Takeuchi and R.-J. Roe, J. Chem. Phys. **94**, 7446 (1991).
[41] E.-G. Kim and W. L. Mattice, J. Chem. Phys. **101**, 6242 (1994).
[42] N. E. Moe and M. D. Ediger, Macromolecules **29**, 5484 (1996).
[43] F. Muller-Plathe, S. C. Rogers, and W. F. v. Gunstern, Macromolecules **25**, 6722 (1992).
[44] P. V. K. Pant and R. H. Boyd, Macromolecules **26**, 679 (1993).
[45] A. A. Gusev, U. W. Suter, and D. J. Moll, Macromolecules **28**, 2582 (1995).
[46] J. A. Young, B. L. Farmer, and J. A. Hinkley, Polymer **40**, 2787 (1999).
[47] *Insight II* (Molecular Simulation Inc., 9865 Scranton Road, San Diego, CA).
[48] A. T. Hagler, E. Huler, and S. Lifson, J. Am. Chem. Soc. **96**, 5319 (1974).
[49] D. H. Kitson and A. T. Hagler, Biochemistry **27**, 5246 (1988).
[50] *Amorphous Cell* (Molecular Simulation Inc., 9865 Scranton Road, San Diego, CA).
[51] H. Meirovitch, J. Chem. Phys. **79**, 502 (1983).
[52] H. Meirovitch, Macromolecules **18**, 569 (1985).
[53] J. M. O'Reilly, J. Polym. Sci. **57**, 429 (1962).
[54] A. Quach and R. Simha, J. Appl. Phys. **42**, 4592 (1971).
[55] O. Olabisi and R. Simha, Macromolecules **8**, 206 (1975).
[56] L. M. Hayden, S. C. Brower, and S. J. Strutz, Macromolecules **30**, 2734 (1997).
[57] W. C. Swope, H. C. Anderson, P. H. Berens, and K. R. Wilson, J. of Chem. Phys. **76**, 637 (1982).
[58] L. V. Woodcock, Chem. Phys. Lett. **10**, 257 (1971).
[59] R. F. Rapold, U. W. Suter, and D. N. Theodorou, Macromol. Theory Simul. **3**, 19 (1994).
[60] R. Zhang and W. L. Mattice, Macromolecules **28**, 7454 (1995).
[61] P. R. Sundararajan, Macromolecules **19**, 415 (1986).
[62] M. Vacatello and P. J. Flory, Macromolecules **19**, 405 (1986).
[63] K. D. Singer, M. G. Kuzyk, and J. E. Sohn, J. Opt. Soc. Am. **4**, 968 (1987).
[64] D. J. Williams, in *Nonlinear Optical Properties of Organic Molecules and*

Crystals, edited by D. S. Chemla and J. Zyss (Academic, New York, 1987), p. 416.
[65] M. A. Pauley, H. W. Guan, and C. H. Wan, J. Chem. Phys. **104**, 6834 (1996).
[66] K. Solc and W. H. Stockmayer, J. Chem. Phys. **54**, 2756 (1971).
[67] K. Solc, J. Chem. Phys. **55**, 355 (1971).
[68] K. Solc, Macromolecules **6**, 378 (1973).
[69] D. N. Theodorou and U. W. Suter, Macromolecules **18**, 1206 (1985).
[70] D. B. Hall, A. Dhinojwala, and J. M. Torkelson, Phys. Rev. Lett. **79**, 103 (1997).